16. Kalybekov T., Rysbekov K., Nauryzbayeva D. Substantiation of averaging the content of mined ores with account of their readiness for mining. *E3S Web of Conferences*. 2020. Vol. 201. 01039. DOI 10.1051/e3sconf/202020101039
17. Bitimbaev M. Zh., Krupnik L. A., Aben Kh. Kh. et al. Adjustment of backfill composition for mineral mining under open pit bottom. *Gornyi Zhurnal*. 2017. No. 2. pp. 57–61. DOI 10.17580/gzh.2017.02.10
18. Krupnik L. A., Bitimbaev M. Zh., Shaposhnik S. N., Shaposhnik Y. N., Demin V. F. Validation of rational backfill technology for Sekisovskoe deposit. *Journal of Mining Science*. 2015. Vol. 51, No. 3, pp. 522–528.
19. Bitimbaev M. Zh. Technological Support for Effective and Integrated Development of Mining and Processing of Mineral Resources in XXI Century (Problems, Prospects, Priorities). Monograph. Almaty : Print House Gerona, 2020. 160 p.
20. Kalybekov T., Rysbekov K. B., Toktarov A. A. et al. Underground mine planning with regard to preparedness of mineral reserves. *GIAB*. 2019. No. 5. pp. 34–43.
21. Makarov A. B. Practical Geomechanics. Textbook for Mining Engineers. Moscow : Gornaya kniga, 2006. 391p.
22. Agoshkov M. I. Classification of mining sciences. Actual problems of development of deposits and use of mineral raw materials. Moscow : MGGU, 1993. pp. 23–30.
23. Puchkov L. A., Zhezhelevskiy Yu. A. Underground mineral mining. Moscow : Gornaya kniga, 2015. Vol. 1. pp. 540–542.
24. Galaev N. Z. Ground control in underground ore mining. Moscow : Nedra, 1990. 100 p.
25. Kozlovskiy E. A. Mining encyclopedia. Moscow : Sovetskaya entsiklopedia, 1989. Vol. 4. pp. 150–153, pp. 301–304.
26. Kazikaev D. M., Savich G. V. Practical course on geomechanics of underground and hybrid ore mining. Tutorial, 2 ed. Moscow : Gornaya kniga, 2013. 224 p.
27. Agoshkov M. I., Malakhov G. M. Underground mining of ore deposits. Moscow : Nedra, 1966. 664 p.
28. Baykonurov O. A. Classification and choice of methods of underground development of deposits. Almaty : Nauka, 1969. 606 p.
29. Shvetsov P. F., Zilberberg A. F., Papernov M. M. Underground space and its development. Moscow : Nauka, 1992. 192 p.
30. Dyadkin Yu. D. The problems of integrated development of subsoil resources and the use of underground space. *Gornyi Zhurnal*. 1990. No. 7. pp. 54–57. EM

UDC 622.7:621.373:622.765

V. A. CHANTURIYA[1], *Chief Researcher, Academician of the Russian Academy of Sciences*
I. Zh. BUNIN[1], *Leading Researcher, Doctor of Engineering Sciences*
M. V. RYAZANTSEVA[1], *Senior Researcher, Candidate of Engineering Sciences, ryzanceva@mail.ru*
I. A. KHABAROVA[1], *Senior Researcher, Candidate of Engineering Sciences*

[1] *Academician Melnikov Institute of Comprehensive Exploitation of Mineral Resources, Russian Academy of Sciences, Moscow, Russia*

EFFECT OF HIGH-POWER ELECTROMAGNETIC PULSES AND DIELECTRIC BARRIER DISCHARGES ON PHYSICOCHEMICAL AND FLOTATION PROPERTIES OF PEROVSKITE

Introduction

By 2018 the global titanium reserves amounted to 872 Mt, including 799.15 Mt of proven titanium dioxide reserves. Russia holds 17.3% of the world's proven reserves occurred in 10 primary deposits (93.4%) and in 10 placers (6.6%) [1]. At the same time, Russia takes only 0.4% in the global production of TiO_2 concentrate. In the meanwhile, the Murmansk Region, alone, holds three titanium–magnetite ore deposits—Kolvitsa, Pudozh and Afrikanda. The largest primary deposits of perovskite–titanomagnetite ore on the Kola Peninsula and in North Karelia contain great reserves of titanium, rare metals (Nb, Ta) and rare earths [2].

Russia's Afrikanda deposit features the largest titanium reserves (the total reserves amount to 52.2 Mt, and the average content of TiO_2 is 9.2%) and represents a promising source of titanium,

The methods of FTIR, SEM–EDX, microhardness test, electrokinetic potential and contact angle measurements, as well as the sorption and flotation experiments are used to study the influence of high-power electromagnetic pulses (HPEMP) and dielectric barrier discharge (DBD) on the structural, physicochemical and flotation properties of perovskite (Afrikanda deposit).

The analysis of FTIR data shows that short treatment times (t_{treat} = 10÷30 s) lead to opposite changes in the surface condition of perovskite: oxidation (hydration) of the surface in case of HPEMP and deoxidizing (dehydration) under DBD.

According to SEM results, the surface of perovskite undergoes destruction as a result of HPEMP and DBD treatment. The surface of some areas of the samples is modified with the formation and opening of deep parallel cracks, most likely due to the polysynthetic twinning typical of perovskite crystals; the subparallel pyramidal protrusions are also observed in some surface areas. The determined morphological changes cause softening and a monotonic decrease in the microhardness of the mineral surface with an increase of the HPEMP and DBD (plasma) treatment times (t_{treat} = 0÷150 s) by ΔHV_{max} = 27÷33%.

The effect of HPEMP and DBD on the physicochemical properties of the mineral surface represents a shift in the electrokinetic potential towards positive values, an increase in the contact angle (t_{treat} = 10÷30 s), as well as the improved adsorption of the collector and the higher flotation activity of perovskite by ~ 10–15%.

Keywords: *perovskite, electromagnetic pulsed discharges, Fourier-transform infrared spectroscopy, scanning electron microscopy, surface modification, microhardness, zeta potential, contact angle, sorption, flotation*

DOI: *10.17580/em.2022.01.09*

rare metals and rare earths [3]. The main useful component—titanium—occurs in perovskite and titanomagnetite; perovskite contains (mass percentage): 0.64–2.50 $(Nb, Ta)_2O_5$, 50.8–56.8 TiO_2, 0.12–1.93 SiO_2, 0.15–1.30 Al_2O_3, 0.43–2.00 Fe_2O_3, up to 1.44 FeO, 2.18–10.7 Ln_2O_3 (sum of REM oxides), 26.3–38.1 CaO, 0.10–2.35 Na_2O, 0.07–0.14 ThO_2 [4, 5].

Perovskite (calcium titanium oxide, formula $CaTiO_3$, chemical composition $(Ca, REE, Na)(Ti, Nb)O_3$ [6]) is a mineral from a large family of perovskites that share a generic formula ABX_3 (where the X position can be taken by such anions as O^{2-}, F^-, Cl^-, Br^-, I^-, $(OH)^-$-groups etc.) Minerals of perovskite group are a small group of accessory minerals that share a formula ABO_3 where the A position is taken by the main cations Ca, Sr, Pb, Ce, La, Nd, Pr, Na, K, Th, U; the B position can be taken by Ti, Nb, Fe, Ta, Zr, with possible isomorphic impurities Al, Si, Mg and Mn [6–9].

Perovskite possesses semiconducting properties, the band gap E_g = ~1.2÷~4 eV, [10], the conductivity type is *n*, the electric conductivity is $\sim 10^{-7}$ $(Ohm \cdot cm)^{-1}$, the thermoelectric coefficient is 7, the carrier concentration is $\sim 4 \cdot 10^{11}$ cm^{-3} [11]; the mineral is paramagnetic, the magnetic susceptibility is $(2.7 \div 13.9) \cdot 10^{-6}$ $emu \cdot g^{-1}$, the density is 3.95–4.2 $g \cdot cm^{-3}$, and the Mohs hardness is 5.5–6 [5].

The processing flowsheet for perovskite–titanomagnetite ore includes a sequence of such operations as [3–5]: crushing, milling, desliming, magnetic concentration of titanomagnetite and calcite flotation of nonmagnetic product; then, washing of reagent in hydrocyclones and perovskite flotation to extract perovskite concentrate with the content of 49–50% TiO_2. Regarding the content of titanium (% by mass: TiO_2—48, CaO—34÷35), the standard perovskite concentrate is similar to the ilmenite concentrate (the common titanium raw material) but the presence of 1–1.2% $(Nb, Ta)_2O_5$ and 3.5–4% La_2O_3 improves the value of the perovskite concentrate as compared with the ilmenite concentrate [3].

Reduction in loss of TiO_2 (with perovskite during desliming, washing and calcite flotation) in marketable concentrates is only achievable with direct selective flotation of perovskite in fresh water with agent IM-50, which ensures concentration of the useful component at the content of 48–50% and recovery of 80–83% from nonmagnetic ore fraction [5, 12, 13].

The complexity of production of a high-quality perovskite concentrate at its high recovery is connected with the similar process properties of perovskite, calcite and olivine.

Application of high-energy effects [11, 14–17] in processing of rebellious minerals enables efficient selective disintegration of finely dissemination mineral aggregates, enhances contrast between the physicochemical and flotation properties of minerals, and improves the further separation thanks to formation of hydrophobic and hydrophilic micro and nano phases on the mineral surface. Pioneering experimental research made it possible to substantiate the mechanism of effect exerted by γ-ray and β-particles on flotation of semiconducting minerals—rutile, ilmenite, ilmenorutile, zircon, chalcopyrite, galenite, perovskite, pyrolusite and antimonite [11]. Radiation-induced defects and reduced concentration of electrons in the surface layer of rutile, ilmenite, chalcopyrite, pyrolusite and antimonite (radiated in water) increased the adsorption of the flotation agent anion on the mineral surface and enhanced the yield of these minerals in flotation on the average by 2–12% (perovskite—by 9%).

Tests proved the intensifying effect of high-power electromagnetic pulses (HPEMP) and dielectric barrier discharge (DBD) cold plasma on acid leaching [14] and flotation [15] of Lovozero eudialyte concentrate, as well as the modifying effect of electromagnetic pulses on the surface structure and physicochemical properties of Juine ilmenite [16] and sulfide minerals and quartz from different deposits [17].

This study aims to analyze and compare the effects produced by the nanosecond electromagnetic pulses and DBD at atmospheric pressure in the air on the surface structure and morphology, microhardness, electrokinetic potential, contact angle, adsorbability and floatability of Afrikanda perovskite with a view to enhancing flotation of complex perovskite–titanomagnetite ore.

Experimental

Testing using procedures [11, 14–18] involved samples of perovskite (formula $CaTiO_3$) in the form of grains extracted from hand specimens of Afrikanda perovskite (Kola Peninsula, Russia) and specially manufactured polished plates approximately 4.5 mm thick. The samples are courtesy of the museum staff members M. Yu. Sidorov, E. A. Selivanova and V. N. Yakovenchuk at the Geological Institute of the Kola Science Center of the Russian Academy of Sciences. The chemical composition and the content of impurities of the samples was determined by the X-ray fluorescence analysis using spectrometer ARL Advant'X (Thermo Fisher Scientific Inc), mass percentage: 48.0 TiO_2, 35.5 CaO, 5.41 SiO_2, 2.15 CeO_2, 1.87 Al_2O_3, 1.62 Fe_2O_3, 0.88 Nb, 1.01 F, 0.65 Nd, 0.55 Na_2O, 0.39 MgO, 0.33 La_2O_3, 0.26 Sr, 0.10 V_2O_5, 0.09 K_2O, 0.08 ZrO_2, 0.05 Sm_2O_3 0.05, Ta_2O_5, 0.04 BaO, 0.03 Y_2O_3, 0.03 Cs_2O, 0.01 Ni, 0.01 Pb, Pr—not detected, Th—not detected.

The details of the electrophysical parameters of electromagnetic treatment (HPEMP and DBD) and the treatment conditions of perovskite samples are given in [14–17]; the treatment duration range is t_{treat} = 10÷150 s. In case of high-power EMP, the front, duration and amplitude of out voltage pulse were ~3–8 ns, 30–50 ns and 70 kV, respectively; the electromagnetic field strength and current in the electrode gap 7 mm long were 10^7 $V \cdot m^{-1}$ and $\sim 10^{11}$ $A \cdot m^{-2}$, respectively [14, 15], the frequency of nanosecond pulses was 375 Hz. For preventing fragmentation of the polished sections and to eliminate dispersion of particles –50 μm in size under high-voltage pulses, the HPEMP treatment conditions for perovskite samples before testing their microhardness, structure and physicochemical properties (electrokinetic potential and contact angle) included the front, duration, out voltage pulse amplitude and pulse repetition rate of 2–5 ns, 4–10 ns, 25–30 kV and 100 Hz, respectively.

For enhancing efficiency of the electromagnetic pulses, the milled samples of perovskite were moistened with distilled water at an S : L ratio of 5 : 1. Then, the samples were placed on a thin dielectric base surface on the side of the grounded electrode. The air gap left between the surface of the top mineral layer and the surface of the active electrode (~0.1–0.2 mm) allowed a periodic spark discharge. After high-voltage EMP treatment, the samples were dried in the air and were kept in the rare atmosphere up to the analysis and flotation tests.

The electrode voltage in DBD generator cell was 20 kV, the pulse duration was 8 μs, the pulse-leading edge duration was 300 ns, the pulse repetition rate was 16 kHz, and the electrode gap was 5 mm long [14–17]. In the conditions of cold nonequilibrium plasma of DBD in the air, the gas temperature in the work zone of the discharge cell was not higher than the dielectric barrier temperature and was at the level of the room

temperature for $t_{treat.}$ = 10÷60 s. The temperature of electrons in micro discharge was a few eV at the electron concentration of 10^{14} cm^{-3} and current density of 10^3 $A{\cdot}cm^{-2}$; the discharge current was varied from 0.1 to 1 mA [16, 17]. Before DBD the samples of perovskite were not moistened.

The change in the surface structure and morphology of perovskite after treatment by electromagnetic pulses was analyzed using the Fourier-transform infrared spectroscopy (FTIR, spectrometer Nicolet-380 (USA) with Smart Diffuse Reflectance) and electron microscopy SEM–EDX, scanning electron microscope LEO 1420 VP with energy-dispersive micro analyzer INCA Energy 350). During the microscopic studies, perovskite grains were fixated on an electroconductive base surface and spattered with thin carbon layer, which prevented from an excessive electric charge.

The IR spectra of perovskite were registered in a range from 4000 cm^{-1} to 400 cm^{-1} (spectral resolution 4–6 cm^{-1}, 100 scans); the intensity of the characteristic lines in the IR spectra varied from spectrum to spectrum, for this reason, the estimate of the relative intensity of the spectrum lines used the ratio of the optical density of each line to the optical density D of line 442–494 cm^{-1}.

The microhardness of the mineral was determined using the Vickers Test (*HV*, MPa; USSR State Standard GOST 2999-75) [15–17]: microhardness tester PMT-3M; the load on the indenter was 100 g, and the loading time was 10–15 s. The flow potential (ζ-potential, mV) of mineral particles (size ≤50 μm) was determined on Microtrac ZETA-Check Zeta Potential Analyzer. The surface contact angle (θ°) of the polished sections before and after energy effects was measured using the drop technique, with a distilled water drop with a diameter of 2–3 mm lying on the flat surface [15–17], with the help of a digital optical microscope and image analysis program ImageJ with DropSnake and LB-ADSA plugins [18].

The procedure of estimating adsorption of a complexing flotation agent—capryl hydroxamic acid [12, 13, 19]—at the surface of perovskite before and after treatment by HPEMP and DBD included agitation of a mineral sample with the agent solutions, filtration of the solid phase, washing, drying of the filtrate and analysis of the mineral surface by the diffuse reflectance infrared Fourier Transform Spectroscopy (spectrometer IRAffinity, Shimadzy with accessory DiffuzIR, Pike Technologies).

Flotation of the test samples (1.0 g, particle size –80+40 μm) was carried out in a flotation cell of 20 ml: the samples were agitated in water for 1 min, then the collector was fed (capryl hydroxamic acid, 200 g/t); the mineral and the agent contact time was 1 min; pH of the medium was brought to 5.5 by adding the aqueous solution of H_2SO_4; after that MIBK was added as a frother to interact with the mineral for 0.5 min; the froth product was separated for 2 min.

Results and Discussion

Fourier Transform Infrared Spectroscopy. The infrared spectrum of perovskite (without treatment by HPEMP or DBD) included lines in the range of 400–800 cm^{-1}, conditioned by variation of structural groups in the crystal lattice of the mineral, and lines in the range of 900–4000 cm^{-1}, connected with the presence of the impurities C–O, O–H, and metal (Me)-O groups localized on the mineral surface [5, 9, 20–22].

The IR spectrum analysis identifies some adsorption band crests as follows: the band crest at 458 cm^{-1} responds with valence vibrations (ν) of the bonds Ti–O–Ti in TiO_2; at 468 cm^{-1} — ν Ti–O–Ti; at 554-570 cm^{-1} — ν Ti–O in TiO_6–octahedrons; at 570 cm^{-1} — ν Ti–O–Ti and Ti–O; at 650–655 cm^{-1} — vibrations of the bond Fe–O in Fe_2O_3; at 655 cm^{-1} — ν Me–O; at 710 cm^{-1} — valence vibrations of the bond ν Ti–O in TiO_6; at 730 cm^{-1} — Ti–O; at 760 cm^{-1} — ν Ti–O–Ti.

In the IR spectrum range of 900–4000 cm^{-1}, the recorded characteristic bands at 906 cm^{-1} and 946 cm^{-1} relate with vibrations of the bond O–O (peroxo-groups); at 931–1338 cm^{-1}—vibrations of the bond Ti–OH; at 1121 cm^{-1}—Fe–OH; at 1413 cm^{-1} responds with the valence vibrations of the bond ν Me–O; at 1415 cm^{-1}—C = O; at 1423 cm^{-1} complies with the symmetrical deformation vibrations of the bond ν C–O; at 1456 cm^{-1}—N–H; at 1460 cm^{-1}—valence vibrations of the bond Me–O. The band at 1650 cm^{-1} stands with the deformation vibrations of the bond d O–H in H_2O (hydroxyl groups disturbed by the hydrogen bond inside the mineral particles); the wide medium-intense band at 3400–3354 cm^{-1} characterizes the valence vibrations of the bond ν O–H in H_2O (free groups of OH on the mineral surface).

For analyzing structural changes of the surface of perovskite under the impact of HPEMP and DBD, four characteristic lines were selected in the infrared spectra of the mineral: at 442–494 cm^{-1} (ν Ti–O–Ti), 632–659 cm^{-1} (ν Me – O), 916–950 cm^{-1} (peroxo-groups –O–O–) and at 1435–1444 cm^{-1} (ν C – O).

As a result of perovskite treatment by HPEMP for t_{treat} = = 30 s, the relative intensity increased in the lines at 632–659 cm^{-1}, 916–950 cm^{-1} and 1435–1444 cm^{-1}, governed by the vibrations of Me–O, –O–O–, and C–O, respectively. Probably, these changes in the infrared spectrum mean oxidation of the surface of pre-moistened perovskite particles under the action of plasma produced by periodic nanosecond high-voltage discharge induced by HPEMP in the air. Simultaneously with oxidation, hydration of perovskite surface takes place, which is identified by the increased intensity in the line at 1616–1693 cm^{-1}, due to the presence of mineral-adsorbed molecules of H_2O (δ O–H in H_2O). Elongation of the pulsed electromagnetic treatment duration to t_{treat} = 50÷150 s naturally causes a local rise in the temperature and, as a consequence, deoxidizing (dehydration) of perovskite surface, which is specified by the decrease in the relative intensity in the lines at 632–659 cm^{-1}, 916–950 cm^{-1} and 1435–1444 cm^{-1}.

The infrared spectra of perovskite treated by dielectric barrier discharge cold plasma change less as compared with the mineral spectra after HPEMP effect. No essential change is observed in the relative intensity in the lines at 916–950 cm^{-1} and 1435–1444 cm^{-1}; some minimal changes in the intensity in these bands are achieved at t_{treat} = 30 s. At the same time, as against variations induced by HPEMP, the noticeable (by 1.2 times) decrease in the intensity is found in the line at 632–659 cm^{-1} (ν Me–O). Probably, as a result of the short-term (t_{treat} = 10–30 s) treatment by DBD, deoxidizing of perovskite surface takes place. Furthermore, DBD treatment for t_{treat} = = 10÷100 s causes reduction in the relative intensity in the line at 1616÷1693 cm^{-1} (bonds δ O–H in H_2O), which responds with dehydration of perovskite surface. The longer duration of plasma treatment up to $t_{treat} \geq 150$ s, both in case of DBD and HPEMP, increases the intensity in this line, which is reflective of intensified hydration of the mineral surface.

Scanning electron microscopy, microhardness testing and physicochemical properties of perovskite. Microstructural defects in perovskite represent mostly the complex curved interfaces of mineral phases formed by

noncrystallographic planes and the slot-like cavities and flaws in perovskite matrix. Optically uniform grains of perovskite are nonuniform in the SEM–BSE images and are composed of two phases (**Fig. 1**): a bright phase **(Prv-I)** having the composition of $(Ca_{0.92}Na_{0.05}(Ce_{0.03}Nd_{0.01})_{0.04})_{1.00}(Ti_{0.95}Fe_{0.03}Nb_{0.02})_{1.00}O_{3.00}$ and a dark phase **(Prv-II)** having the composition of $(Ca_{0.96}Na_{0.02}(Ce_{0.02}Nd_{0.01})_{0.03})_{1.01}(Ti_{0.97}Fe_{0.02}Nb_{0.01})_{1.00}O_{3.01}$. The interfaces of these phases are complex, curved, noncrystallographic, probably epigenetic, connected with the redistribution of the components in metasomatic recrystallization, as a result of which perovskite undergoes accumulation of loparite $NaCe(Ti,Nb)_2O_6$, increase in the contents of Na and REE, and redistribution of Th and Nb. The slot-like cavities between the zonal grains of perovskite are filled with calcite and silicates (maize-yellow titanite Tit-$CaTiSiO_5$ with impurities of Al and Fe, and with brithilite-(Ce) (Brt)—silicophosphate of rare earths $Ca_2(Ce, Ca)_3[(OH, F)|(SiO_4, PO_4)_3]$) (see Fig. 1*a*). Moreover, the cavities contain coarse grains of pyrite, completely replaced by micro cryptocrystallitic aggregates of iron hydroxides (limonite $FeOOH{\cdot}(Fe_2O_3{\cdot}nH_2O)$ (see Fig. 1*b*). Rare earth carbonates from ancylite group fill the finest flaws which grow through the whole volume of perovskite: these are ancylite-(Ce) having the composition of $(Sr_{0.53}Ca_{0.47})_{1.00}(Ce_{0.50}La_{0.32}Nd_{0.12}Pr_{0.06})_{1.00}[CO_{3.00}]_{2.00}(OH){\times}H_2O$ and calcioancylite-(Ce) having the composition of $(Ca_{0.70}Sr_{0.30})_{1.00}(Ce_{0.52}La_{0.28}Nd_{0.15}Pr_{0.05})_{1.00}[CO_{3.00}]_{2.00}(OH){\times}H_2O$.

By the data of SEM–EDX, the high-voltage nanosecond pulses induce failure of perovskite structure and modify the surface in some areas of the test samples (**Fig. 2**). In particular, deep parallel cracks appear (see Fig. 2*a*), which are, probably, the consequence of polysynthetic twinning typical of crystals of perovskite. There are also surface areas formed by subparallel pyramidal spikes (see Fig. 2*b*).

Nonthermal HPEMP treatment softens the mineral surface; microhardness of perovskite decreases with longer time of treatment from 930 MPa in the initial state to 624 MPa at t_{treat} = 150 s, i.e. ΔHV_{max} = 33%. Under short-term pulses (t_{treat} = 30 s), microhardness also decreases (*HV* = 748 MPa; ΔHV = 20%).

The changes in the surface morphology of perovskite treated by DBD (t_{treat} = 50 s) are connected with the defects in the form of inter-grain and intra-grain cracks (Fig. 2*c*) and, similarly to HPEMP, pyramidal spikes on the surface (Fig. 2*d*).

As a result of the action exerted by strong electric field, micro discharge, ozone and chemically active particles generated in the dielectric barrier discharge plasma [17, 23], the surface of the test perovskite samples softens and their microhardness decreases with the longer treatment time from *HV* = 912 to 663 MPa at t_{treat} = 0 and 150 s, respectively. In this manner, the short-term (t_{treat} = 10÷30 s) electromagnetic pulses are effective both in disintegration (formation of micro cracks and unsaturated chemical bonds) and in modification of surface structure of perovskite.

The electrokinetic potential of perovskite changes nonlinearly (nongradually) subject to time of the pulsed electromagnetic treatment. As a result of short-term (t_{treat} = 10÷50 s) impact of HPEMP, the negative values of the electrokinetic potential decrease from –85.4 mV (t_{treat} = 0 s) to –83.9 mV and –77.2 mV at t_{treat} = 10 and 50 s, respectively. Under the impact of DBD, the potential gradually decreases to –77.5 mV at t_{treat} = 10 s and to –75.4 mV at t_{treat} = 50 s.

With increasing duration of the pulsed electromagnetic treatment (both in case of HPEMP and DBD), the contact angle Q of perovskite surface changes nongradually: at t_{treat} = 30 s, it increases from 75° (t_{treat} = 0 s) to 80.5° (HPEMP) and 77.5° (DBD). Probably, the found effect of the increased hydrophobic behavior of the mineral surface as a result of the short-term (t_{treat} = 10–30 s) energy deposition can improve the adsorption and flotation properties of the mineral. The proved changes in microhardness, electrokinetic potential and contact angle of perovskite surface agree with the experimental data obtained for eudialyte [15] and ilmenite [16].

Adsorption and flotation properties of perovskite. The FTIR spectroscopy proved that the short-term (t_{treat} = 10 s) treatment of eudialyte by HPEMP and DBD improved adsorption of agent Flotinor at the mineral surface [15]. Moreover, it was found that the adsorbability of eudialyte relative to the collecting agent (sodium oleate) was improved when NaOl was combined with a regulating agent (sodium sulfate Na_2SO_3) thanks to the preliminary pulsed electromagnetic treatment (HPEMP) of the mineral particles at t_{treat} = 10÷100 s [15]. In all tests with HPEMP and DBD, the decrease in the negative electrokinetic potential of eudialyte resulted in the increased adsorption of the anionic collector and consequently, in the increased extraction of eudialyte in flotation concentrate [15].

The spectral curves of the initial and treated (by HPEMP and DBD) samples of perovskite are shown in **Fig. 3**.

The spectral analysis reveals some features in the profiles of diffusive reflectance IR spectra of micro powdered perovskite, which characterize the mechanism of the agent adsorption at the mineral surface. In the spectrum of the initial sample (t_{treat} = 0 s), there is a series of bands which describe attachment of capryl hydroxamic acid at perovskite surface: absorption at 2850 cm^{-1} and 2930 cm^{-1}—valence vibrations in the bond C–H of satisfied hydrocarbons; the bonds at 1510 cm^{-1} and 1550 cm^{-1} characterize complexing with titanium, and the bond at 1610 cm^{-1} is reflective of physisorption of hydroxamic acid.

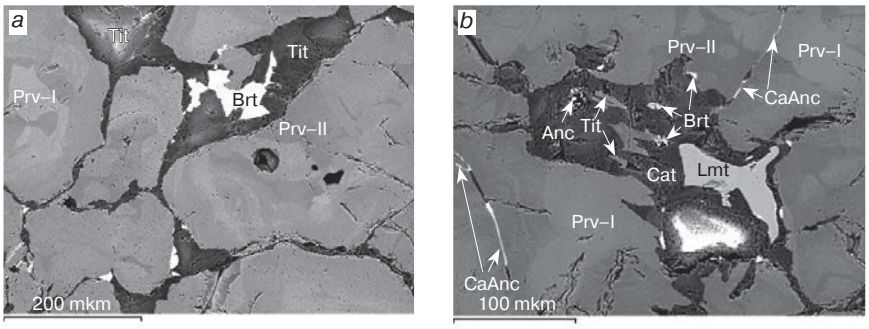

Fig. 1. (*a*) SEM (BSE) image of perovskite surface: two phases in perovskite grains (Prv-I, with REE, and Prv-II), britholite-(Ce) (Brt) and titanite (Tit); (*b*) ameboid grain of limonitic pyrite (Lmt) in the cavity filled with calcite (Cal), titanite (Tit), britholite-(Ce) (Brt), calcioancylite-(Ce) (CaAnc) and ancylite-(Ce) (Anc)

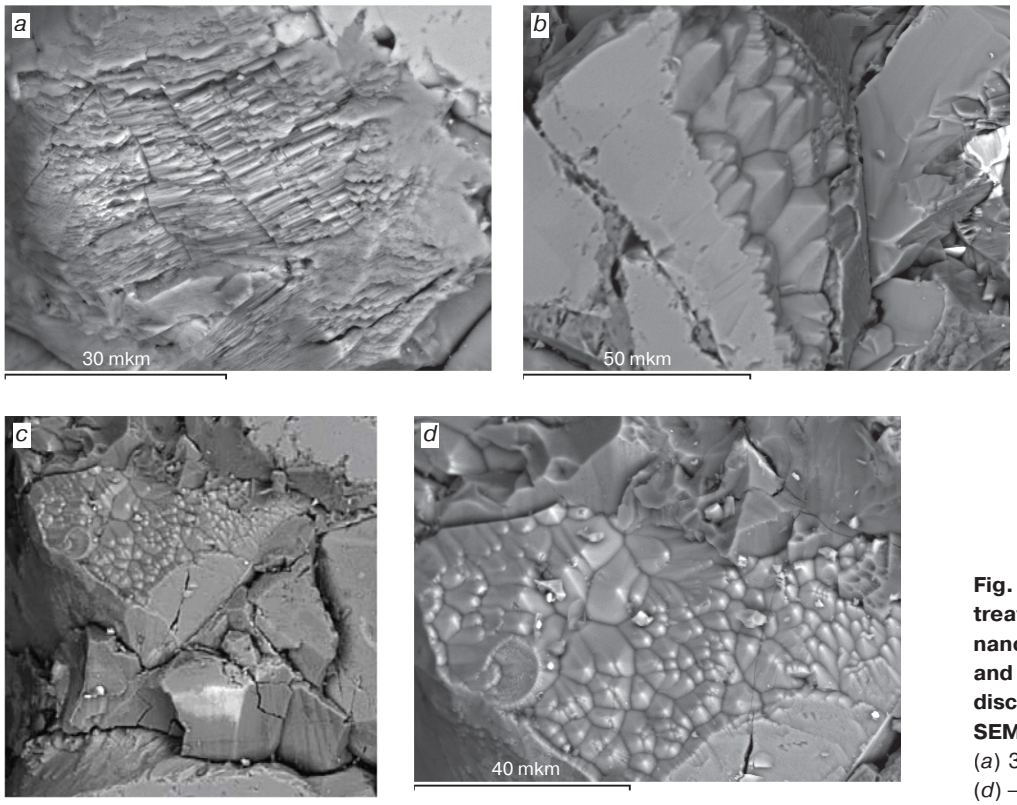

Fig. 2. Perovskite surface after treatment by (*a*), (*b*) high-voltage nanosecond pulses (HPEMP) and by (*c*), (*d*) dielectric barrier discharge (DBD) ($t_{treat.}$ = 50 s). SEM; bevel scales:
(*a*) 30, (*b*) 50, (*c*) 100, (*d*) 40 mm. (*d*) – fragment (*c*)

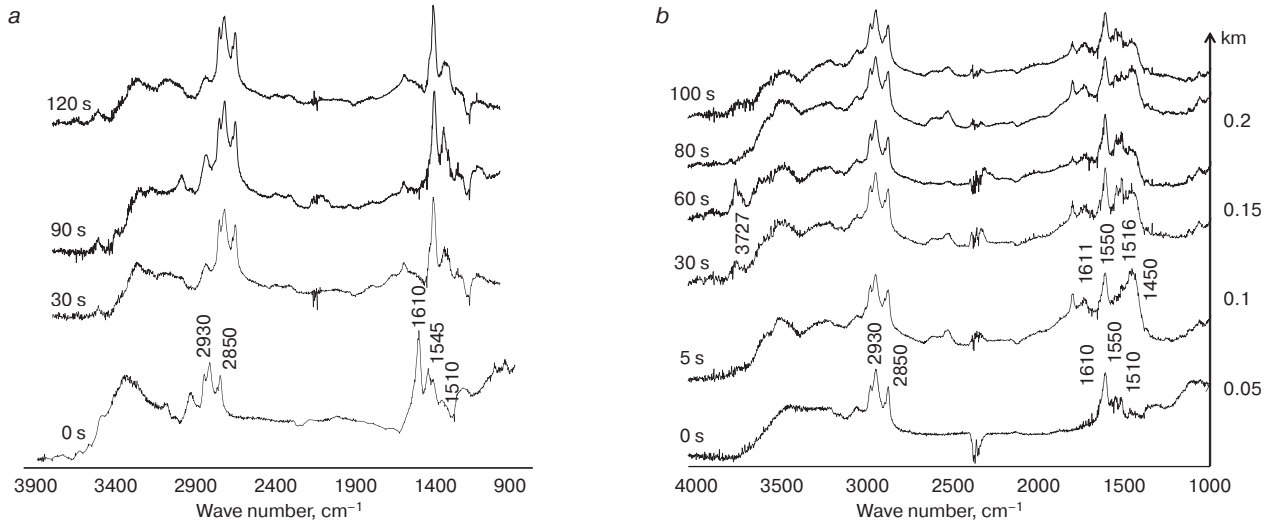

Fig. 3. Effect of electromagnetic pulses on adsorption activity of perovskite surface relative to collecting agent (capryl hydroxamic acid):
(*a*) high-power electromagnetic pulses (HPEMP); (*b*) dielectric barrier discharge (DBD); $t_{treat.}$ = 0–150 s

The spectral curves of the HPEMP-treated samples ($U_a \cong 70$ kV) have a similar set of crests but the integral intensities of the bands related to the adsorbed collector increase by 1.1–1.2 times as compared with the initial sample (see Fig. 3*a*).

The DBD treatment of perovskite induces some essential changes in the IR spectra (see Fig. 3*b*): additional bonds appear at 1450 cm^{-1} and 1516 cm^{-1} integral intensity grows in the spectrum range of 1180–2130 cm^{-1}, which points at the increased adsorption activity of the mineral surface relative to capryl hydroxamic acid. The bond at 1516 cm^{-1}, probably, is reflective of the fact that the main form of the reagent attachment at the DBD-modified mineral surface is the complex compound of hydroxamic titanium [5].

Considering the test data on modifying effect exerted by the pulsed electromagnetic discharges on the physicochemical properties of perovskite, namely, the decrease in the negative values of the electrokinetic potential of the mineral (shift towards positive values), the increase in the contact angle and the improved adsorption of the collector, it was decided to analyze the influence of HPEMP (t_{treat} = 60÷120 s) and DBD

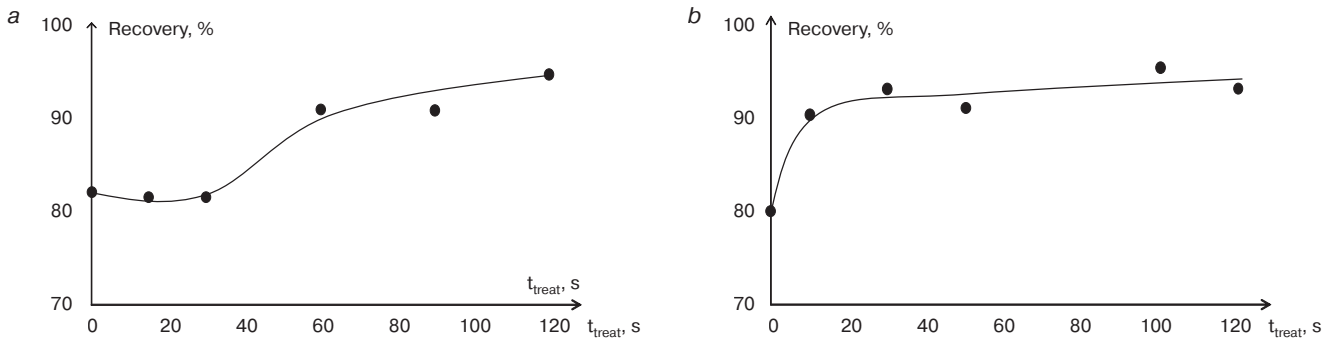

Fig. 4. Effect of (*a*) HPEMP and (*b*) DBD on flotation activity of perovskite

(t_{treat} = 10÷150 s) on floatability of the mineral with capryl hydroxamic acid.

After preliminary electromagnetic treatment (HPEMP and DBD), owing to the change in the structure and chemistry of the mineral surface, enhanced hydrophobic behavior and improved adsorbability, the total extraction of monomineral fraction of perovskite in flotation froth grows by ~10–15%: HPEMP—ε ≅ 90% (t_{treat} = 60 s) and ~95% (t_{treat} = 120 s) (**Fig. 4*a***); DBD—ε ≅ 90÷93% (t_{treat} = 10÷30 s) and ε ≅ 95% (t_{treat} = 100 s) (**Fig. 4*b***). The determined parameters of energy effects and the reagent regime of flotation can be used to stimulate flotation efficiency of perovskite ore of Afrikanda deposit.

Conclusions

The analysis of the data on spectroscopy (FTIR) and scanning electron microscopy has proved the effect of the pulsed electromagnetic and electric discharge (HPEMP, DBD) treatment on the surface structure, morphology, microhardness, physicochemical and flotation properties of Afrikanda perovskite. Appearingly, the structural changes of the mineral surface under impact (t_{treat} = 10÷30 s) of high-voltage electric fields of high-power nanosecond electromagnetic pulse (HPEMP) and dielectric barrier discharge (DBD) in the air are conditioned by oxidation (hydration) of the surface (in case of HPEMP) and, vice versa, by deoxidizing (dehydration) of the surface (in case of DBD).

The morphological changes of the mineral surface represent deep parallel cracks which appear as a consequence of polysynthetic twinning typical of perovskite crystals, and subparallel pyramidal spikes produced by energy deposition. These defects induce softening of the mineral surface and monotonous decrease in its microhardness with longer time of the electromagnetic and cold plasma treatment on the whole by ΔHV_{max} = 27÷33%.

The tests have proved the modifying effect exerted by HPEMP and DBD on the physicochemical properties of the mineral, represented by the shift of the electrokinetic potential towards the positive values, by the increase in the contact angle at t_{treat} = 10÷30 s and by the improved adsorption of the collecting agent, which enhances floatability and total extraction of monomineral fraction of perovskite in flotation froth by ~ 10–15%.

Acknowledgments

The authors express their gratitude to Candidate of Geological and Mineralogical Sciences E.V. Koporulina and to Candidate of Engineering Sciences N.E. Anashkina for their help in the experimentation.

The study was supported by the Ministry of Science and Higher Education of the Russian Federation, Project No. 13.1902.21.0018, Agreement No. 075-15-2020-802.

References

1. Zanolotskaya Yu. V., Sadyhov G. B., Tuzhilina A. S. The promising nature of hydrometallurgical autoclave leaching by lime milk in integrated processing of silica-titanium concentrates. *Plaksin's Lectures-2021 : Eco-Safe and Integrated Processing of Natural Minerals and Mining Waste. Collected Papers.* Vladikavkaz : SKGMI (GTU), 2021. pp. 440–442.
2. Sokolov S. V. Perovskite and titanite—potential nonconventional sources of titanium : A case-study of Afrikanda Deposit. *Plaksin's Lectures-2021 : Innovations in Integrated Processing of Natural Minerals and Mining Waste. Collected Papers.* Apatity : FITS KNTS RAN, 2020. pp. 95–97.
3. Nikolaev A. I., Larichkin F. D., Luhton M. M. Problems of integrated re-appraisal and mining of Afrikanda perovskite–titanomagnetite ore deposit. *Gornyi Zhurnal*. 2003. No. 11. pp. 10–14.
4. Nikolaev A. I. Use prospects of Afrikanda perovskite ore. *SEVER promyshlennyi.* 2007. No. 8.
5. Naifhonov T. B., Beloborodov V. I., Zakharova I. B. Flotation of complex titanium and zirconium ores. Apatity : KNC RAN, 1994. 155 p.
6. Mitchell R. H., Welch M. D., Chakhmouradian A. R. Nomenclature of the perovskite supergroup: A hierarchical system of classification based on crystal structure and composition. *Mineralogical Magazine*. 2017. Vol. 81, No. 3. pp. 411–461.
7. Popova E. A. Crystal chemistry and physical properties of minerals and synthetic compounds having perovskite-type structure : Thesis of Dissertation of Candidate of Geologo-Mineralogical Sciences. Saint-Petersburg : SPbGU, 2018. 354 p.
8. Syrov E. V. Synthesis, structure and physicochemical properties of niobates having structure of laminated perovskite : Thesis of Dissertation of Candidate of Chemical Sciences. Nizhniy Novgorod : NNGU, 2021. 138 p.
9. Mitchell R. H. Perovskites: Modern and Ancient. Ontario, Canada : Almaz Press Inc., 2002. 316 p.
10. Xiao Z., Zhou Y., Hosono H. et al. Bandgap optimization of perovskite semiconductors for photovoltaic applications. *Chemistry – A European Journal.* 2018. Vol. 24. pp. 2305–2316.
11. Shafeev R. Sh., Chanturiya V. A., Yakushkin V. P. Ionizing radiation effect on flotation. Moscow : Nauka, 1971. 58 p.
12. Zheng Y., Cui Y., Wang W. Activation mechanism of lead ions in perovskite flotation with octyl hydroxamic acid collector. *Minerals*. 2018. Vol. 8(8). DOI: 10.3390/min8080341

13. Wang W., Zhu Y., Zhang S. et al. Flotation behaviors of perovskite, titanaugite, and magnesium aluminate spinel using octyl hydroxamic acid as the collector. *Minerals.* 2017. Vol. 7(8). DOI: 10.3390/MIN7080134
14. Bunin I. Zh., Ryazantseva M. V., Minenko V. G. et al. Effects of massive electromagnetic pulses on the structural and chemical properties and leaching efficiency of eudialyte concentrate. *Obogashchenie Rud*. 2021. No. 5. pp. 10–15. DOI: 10.17580/or.2021.05.03
15. Chanturiya V. A., Bunin I. Zh., Ryazantseva M. V. et al. Effect of electromagnetic pulses on structural, physicochemical and flotation properties of eudialyte. *Journal of Mining Science.* 2021. Vol. 57(1). pp. 96–105.
16. Bunin I. Zh., Chanturiya V. A., Anashkina N. E. et al. Effect of high-voltage nanosecond pulses and dielectric barrier discharges on the structural state and physicochemical properties of ilmenite surfaces. *Bulletin of the Russian Academy of Sciences Physics.* 2021. Vol. 85(9). pp. 974–978.
17. Bunin I. Zh., Chanturiya V. A., Ryazantseva M. V. et al. Changes in the surface morphology, microhardness, and physicochemical properties of natural minerals under the influence of a dielectric barrier discharge. *Bulletin of the Russian Academy of Science.* 2020. Vol. 84(9). pp. 1161–1164.
18. Stalder A. F., Melchior T., Muller M. et al. Low-bond axisymmetric drop shape analysis for surface tension and contact angle measurements of sessile drops. *Colloids and Surfaces A : Physicochemical and Engineering Aspects*. 2010. Vol. 364(1-3). pp. 72–81.
19. Mitrofanova G. V., Chernousenko E. V., Kameneva Yu. S. et al. Testing of a complexing reagent on the basis of hydroxamic acids by floating transition metal minerals. *HERALD of the Kola Science Centre of RAS*. 2019. Vol. 11(2). pp. 95–104.
20. Karthikeyan C., Thamima M., Karuppuchamy S. Dye removal efficiency of perovskite structured $CaTiO_3$ nanospheres prepared by microwave assisted method. *Materials Today Proceedings.* 2019. Vol. 35. pp. 44–47.
21. Stoyanova D., Stambolova I., Blaskov V. et al. Mechanical milling of hydrothermally obtained $CaTiO_3$ powders-morphology and photocatalytic activity. *Nano-Structures & Nano-Objects.* 2019. Vol. 18. DOI:10.1016/j.nanoso.2019.100301
22. Nakamoto K. Infrared and Raman Spectra of Inorganic and Coordination Compounds. Part A: Theory and Applications in Inorganic Chemistry, Sixth Edition. John Wiley & Son, 2008.
23. Lazukin A. V., Grabelnykh O. I., Serdyukov Yu. A. et al. The effect of surface barrier discharge plasma products on the germination of cereals. *Technical Physics Letters.* 2019. Vol. 45(2). pp. 16–19. EM

UDC 622.7

A. A. LAVRINENKO[1], *Head of Laboratory, Doctor of Engineering Sciences, lavrin_a@mail.ru*
P. A. SYSA[1], *Senior Researcher, Candidate of Engineering Sciences*
I. I. AGARKOV[1], *Post-Graduate Student*

[1] *Institute of Comprehensive Exploitation of Mineral Resources Russian Academy of Sciences, Moscow, Russia*

HIGH-EFFECTIVE MAGNETIC HYDROCYCLONING EQUIPMENT FOR MAGNETITE ORE PROCESSING

A new method and equipment for magnetic hydrocycloning are proposed, which make it possible to extract the magnetic fraction from a polydisperse suspension with a high specific productivity and separation efficiency without preliminary classification by size.

An alternating magnetic field source is coaxially superimposed on top of the hydrocyclone so that the magnet-like lines intersect the suspension flow rotating in the cylindrical part of the hydrocyclone. In this case, the gradient of the magnetic field inside the body of the hydrocyclone is directed opposite to the direction of the summed vectors of the centrifugal force and gravitational force, and the magnetic fraction (product) is redirected through a drain tube for the concentrate outlet. It is possible to adjust the operating mode of the magnetic hydrocyclone for adjusting the total area of the outlet holes in the drain tube by moving an insert with slot-like cuts, which changes the overlap area of the holes.

The magnetic hydrocyclone is recommended for processing ferruginous quartzite and other types of ores with pronounced magnetic properties. The results of the effective separation of magnetic and nonmagnetic particles at different magnetic field densities are presented, and the dependence of the magnetic fraction recovery on the size of the initial suspension feed is described.

A method is proposed for estimating the possibility of extracting magnetic particles at preset parameters, for example, the geometric dimensions of the magnetic hydrocyclones at the varied values of the magnetic field density and particle flow velocity. The formula for the calculation is given, which establishes the equality, when the particle overcomes the internal space of the hydrocyclone and is extracted into the concentrate.

Keywords: *magnetic hydrocyclone, separation selectivity, magnetic fraction, iron ore beneficiation, magnetic force, centrifugal force, iron content*

DOI: *10.17580/em.2022.01.10*

Introduction

The annual output of iron-bearing ore processing in Russia exceed 200 Mt, which calls for continuous improvement and effectivization of processing process charts, technologies and equipment. The highest expenses in mineral mining and processing are connected with mineral milling and dissociation. Milling is interlinked with hydraulic sizing of mill flows within the mill–sizer circuit. The sizer gives coarse particles which may contain dissociated iron back to the mill, which implicates losses of the overground magnetic mineral with fines in the circuit of magnetic concentration. In his time, P. E. Ostapenko proposed to replace sizes by magnetic separators as in that case the re-milling circuit obtained the coarse aggregates with the lowest content of iron. Thus, the identified problem necessitates engineering of a machine capable to combine the functions of hydraulic sizing and magnetic separation [1].